Fundamental exciton linewidth broadening in monolayer transition metal dichalcogenides

Garima Gupta and Kausik Majumdar*
Department of Electrical Communication Engineering, Indian Institute of Science, Bangalore 560012, India

(Received 13 September 2018; revised manuscript received 18 January 2019; published 8 February 2019)

Monolayer transition metal dichalcogenides (TMDS) are highly luminescent materials despite being sub-nanometer thick. This is due to the ultrashort (<1 ps) radiative lifetime of the strongly bound bright excitons hosted by these materials. The intrinsically short radiative lifetime results in a large broadening in the exciton band with a magnitude that is about two orders greater than the spread of the light cone itself. The situation calls for a need to revisit the conventional light cone picture. We present a modified light cone concept which places the light line ($\hbar cQ$) as the generalized lower bound for allowed radiative recombination. A self-consistent methodology, which becomes crucial upon inclusion of large radiative broadening in the exciton band, is proposed to segregate the radiative and the nonradiative components of the homogeneous exciton linewidth. We estimate a fundamental radiative linewidth of 1.54 ± 0.17 meV, owing purely to finite radiative lifetime in the absence of nonradiative dephasing processes. As a direct consequence of the large radiative limit, we find a surprisingly large ($\sim$0.27 meV) linewidth broadening due to zero-point energy of acoustic phonons. This obscures the precise experimental determination of the intrinsic radiative linewidth and sets a fundamental limit on the nonradiative linewidth broadening at $T = 0$ K.

DOI: 10.1103/PhysRevB.99.085412

I. INTRODUCTION

Monolayers of transition metal dichalcogenides (TMDs, for example, MoS_2, $MoSe_2$, WS_2, and WSe_2) host a unique class of strongly bound two-dimensional excitons [1–3] with a large binding energy of about 500 meV [1,4–7]. This has attracted significant interest from the researchers, and a wide variety of excitonic complexes and their manipulations have been reported in the recent past [8–10]. Interestingly, these excitons exhibit ultrashort radiative lifetime ($\tau_r < 1$ ps) [11–14], which is orders of magnitude shorter than that of conventional semiconducting light emitters including III-V semiconductors like GaAs, InGaAs [15–17], II-VI semiconductors like CdSe and their quantum dots [17–19], organic semiconductors [20], and carbon nanotubes [21–23]. Such a fast radiative-decay manifests as strong photoluminescence [24,25] and electroluminescence [26,27] exhibited by the monolayers of these materials. This makes these ultrathin, flexible, photoactive crystalline sheets an excellent candidate for a plethora of light emitting applications. A deep insight into the fundamental limits of the radiative excitonic decay in these materials is thus essential to exploit the full potential of the short-lived excitons.

One inevitable consequence of the ultrashort radiative lifetime is the large homogeneous broadening (of about 1–2 meV) of the excitonic states due to Heisenberg's uncertainty principle. This broadening is more than two orders of magnitude larger than the total energy extent of the conventional light cone in the exciton band structure. This suggests a need to revisit our understanding of the light cone in such systems. In this work, we propose a generalization of the light cone picture to address two fundamental homogeneous broadening mechanisms that determine the lowest achievable excitonic emission linewidth in an experiment, namely: (1) radiative broadening due to ultrashort spontaneous emission lifetime and (2) nonradiative broadening due to zero-point energy of phonons. To address these limiting scenarios, we use a combination of theory and temperature dependent photoluminescence data from high quality monolayer $MoSe_2$ samples. The limits, as imposed by the aforementioned governing mechanisms on the homogeneous linewidth, are estimated to be $\Gamma_{\mathrm{hom},R} = 1.54 \pm 0.17$ meV and $\Gamma_{\mathrm{NR}}(T = 0) \approx 0.27$ meV, respectively. This is obtained using a self-consistent approach that correlates the microscopic exciton band broadening with the experimental data.

II. REVISITING THE CONCEPT OF LIGHT CONE FOR EXCITONS IN MONOLAYER TMDS

The radiative linewidth of 1s exciton photoluminescence peak in monolayer TMDs has been reported to be on the order of 1–2 meV [28–30]—a manifestation of fast spontaneous radiative recombination. It is instructive to include this radiative lifetime induced large fundamental broadening of the excitonic states and also contributions from other dephasing mechanisms within the existing light cone understanding. The idea of the conventional light cone in the case of infinite exciton lifetime is the following: For the monolayers of Mo based materials, we only consider contribution from the spin allowed bright transition between the topmost valence band v and the lowermost conduction band c and the around the $\mathbf{K}, \mathbf{K}'$ points in the Brillouin zone [see Fig. 1(a)]. We solve the two-particle exciton Hamiltonian in the Bethe-Salpeter (BS) formalism to obtain the exciton band dispersion with the center of mass (COM) momentum $\mathbf{Q} = \mathbf{k_e} + \mathbf{k_h}$ [31,32]. The

*kausikm@iisc.ac.in

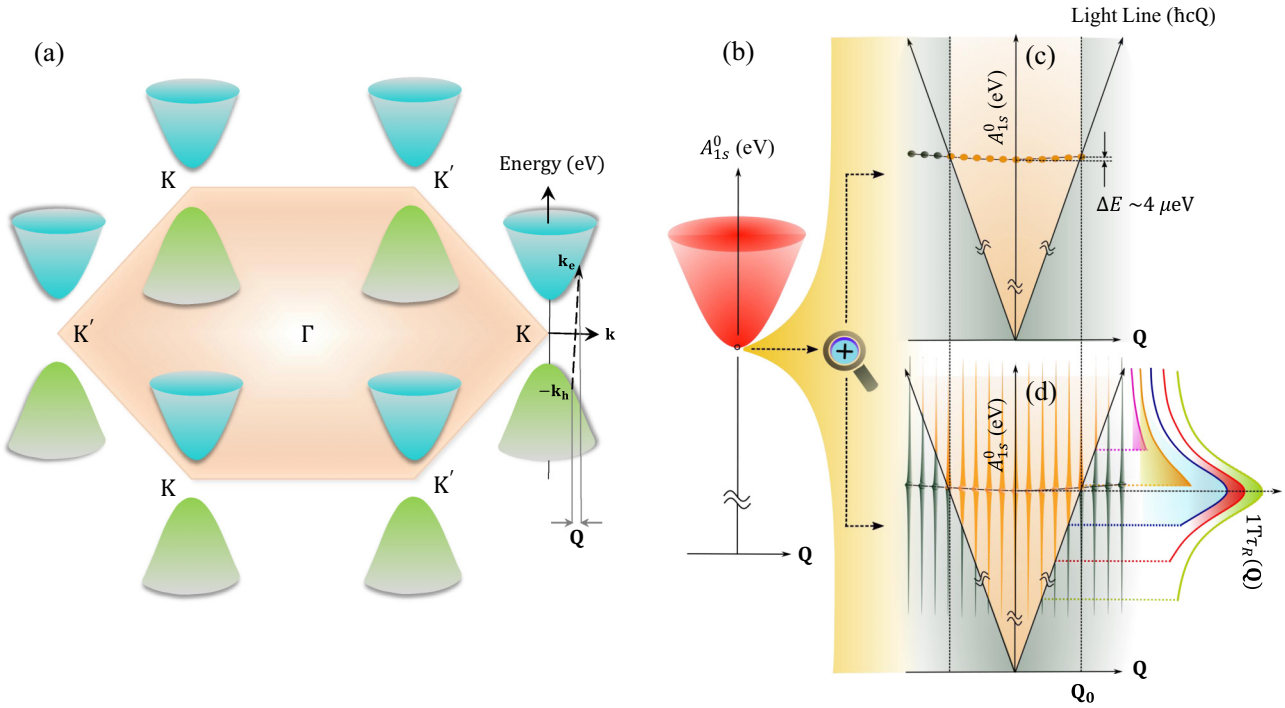

FIG. 1. Modified light cone for exciton bands with large broadening in monolayer TMDs. (a) Electronic band structure of monolayer $MoSe_2$ around the Brillouin zone corners $\mathbf{K}, \mathbf{K}'$, showing the spin allowed bright transition from the uppermost valence band v (in green) to the lowermost conduction band c (in blue) on absorbing a photon. Here $\mathbf{k}$ denotes the quasiparticle momentum. (b) Energy dispersion of the A^0_{1s} exciton with its center of mass momentum ($\mathbf{Q}$). The conventional light cone for the A^0_{1s} exciton shown as zoomed in (c). (c) The radiatively bright exciton states within the light cone are shown as orange dots, while the dark states outside the light cone are represented by grey dots. The demarcation between the two is the light cone boundary $\mathbf{Q_0}$. The extent of the light cone is $\Delta E = E_{1s}(\mathbf{Q_0}) - E_{1s}(\mathbf{0}) \sim 4\,\mu$eV, which is approximately two orders of magnitude smaller than the intrinsic radiative linewidth limit of excitons, which is typically on the order of 1–2 meV. (d) The modified light cone showing the large broadening of the excitonic states. The photon energy $\hbar c$Q (Light Line) due to its in-plane component of momentum is the lower bound on the exciton energy for light emission, i.e., excitons with energy $E_{1s}(\mathbf{Q}) \geqslant \hbar c$Q will emit a photon upon recombination. This extends the conventional light cone beyond $\mathbf{Q_0}$. (Right panel) Decay rate variation of excitons with energy at different $\mathbf{Q}$.

state $|\Psi_s(\mathbf{Q})\rangle$, which denotes an exciton state occupying band s at a characteristic momentum $\mathbf{Q}$, can be expanded in the basis of single electron and hole states in the reciprocal space as

$$|\Psi_s(\mathbf{Q})\rangle = \sum_{v,c,\mathbf{k}} \lambda^{(s)}_{\mathbf{Q}}(\mathbf{k}) |v, \mathbf{k}\rangle\, |c, \mathbf{k}+\mathbf{Q}\rangle. \tag{1}$$

The lowest energy A^0_{1s} exciton band is schematically illustrated in Fig. 1(b). On zooming we get Fig. 1(c), showing that only a small fraction of the states in the band are radiatively bright; the demarcation between the allowed and prohibited states for radiative recombination is determined by the light cone boundary $\mathbf{Q_0}$ ($\mathbf{Q_0} : E_{1s}(\mathbf{Q_0}) = \hbar c Q_0$). Owing to the energy and in-plane momentum conservation between the recombining exciton and the emitted photon, the states lying at $\mathbf{Q} > \mathbf{Q_0}$ are radiatively dark, as the out-of-plane component of the momentum of the emitted photons by these excitonic states ceases to be a real value.

The energy extent of the light cone is roughly given by $\Delta E = \hbar^2 Q_0^2/2m_{\text{ex}} \sim 4\ \mu$eV [Fig. 1(c)] ($\hbar$ is the reduced Planck constant and m_{ex} is the exciton mass), which is almost two orders of magnitude smaller than the exciton linewidth closest to the homogeneous limit as reported by Cadiz *et al.* [29] and Ajayi *et al.* [28]. This mismatch is schematically illustrated in Fig. 1(d), where the large broadening of the discrete exciton states in the dispersion curve is explicitly shown. This is in stark contrast with Fig. 1(c), which is valid only when the exciton lifetime is very large. The light cone determined radiative boundary now undergoes a modification due to exciton state broadening, extending beyond $\mathbf{Q_0}$. An exciton of energy $E_{\text{ex}}(\mathbf{Q})$ emits a photon with out-of-plane component of momentum $q_z = \sqrt{(E_{\text{ex}}(\mathbf{Q})/\hbar c)^2 - Q^2}$, which is a real quantity provided $E_{\text{ex}}(\mathbf{Q}) \geqslant \hbar c Q$. Hence, the photon dispersion due to its in-plane momentum $\hbar c Q$ (light line) is the lower bound energy for allowed radiative transition of excitons at $\mathbf{Q}$. Figure 1(d) is a general light cone diagram in TMDs, in which a nonzero fraction of states at $\mathbf{Q} > \mathbf{Q_0}$ are radiatively active depending on the extent of the broadening, which are otherwise assumed to be forbidden for the conventional light cone in Fig. 1(c).

III. EXPERIMENT

We mechanically exfoliate monolayers of $MoSe_2$ on a clean Si substrate covered with 285-nm thick SiO_2. Photoluminescence measurement is carried out by varying the sample temperature from 3.2 to 220 K. The pressure of the sample chamber is kept below 10^{-4} Torr at all measurement

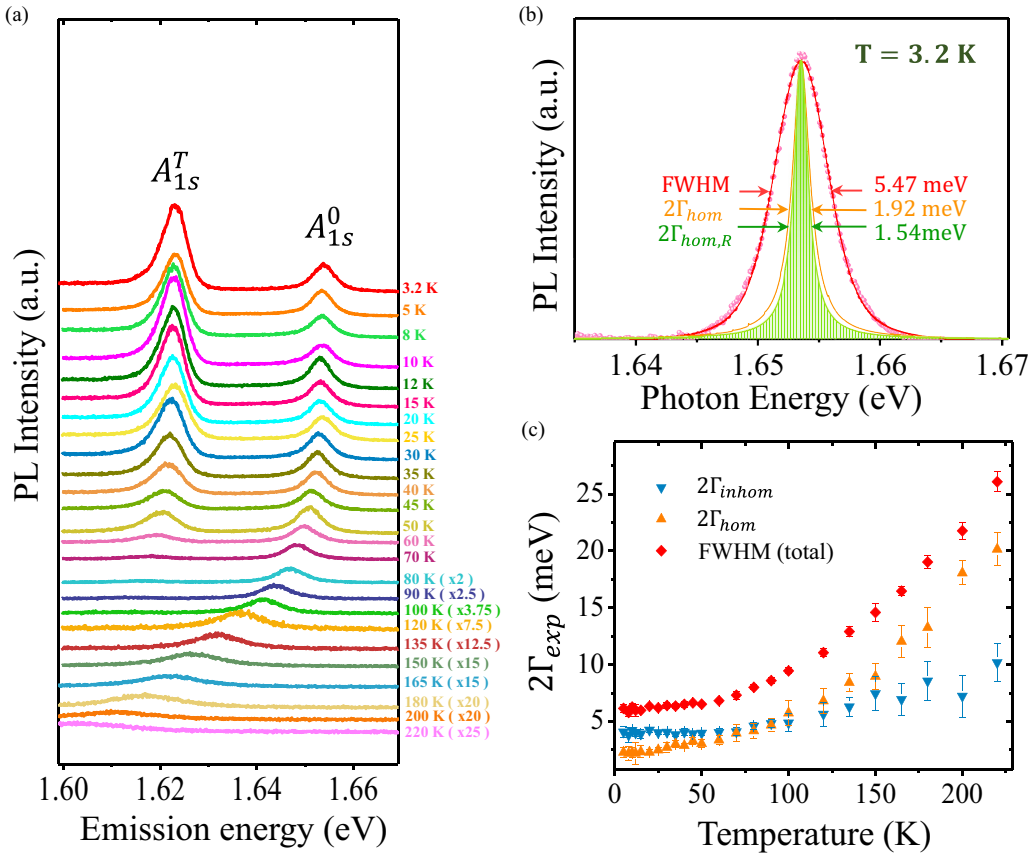

FIG. 2. Photoluminescence linewidth of monolayer $MoSe_2$. (a) Acquired photoluminescence spectra of monolayer $MoSe_2$ on SiO_2 substrate showing the 1 s neutral exciton (A^0_{1s}) and trion (A^T_{1s}) peaks as the sample temperature varies from 3.2 to 220 K. (b) The experimental A^0_{1s} spectrum (in symbols) with an FWHM = 5.47 meV, the fitted Voigt function (in red line), and the deconvoluted Lorentzian with linewidth of $2\Gamma_{\rm hom} = 1.92$ meV (in orange) at $T = 3.2$ K. The patterned filled curve (in green) is the simulated PL spectrum with broadening equal to the fundamental radiative linewidth of $2\Gamma_{{\rm hom},R} = 1.54$ meV. (c) Temperature dependence of the extracted A^0_{1s} exciton linewidth (FWHM) and its constituent Gaussian (inhomogeneous) $2\Gamma_{\rm inhom}$ and Lorentzian (homogeneous) $2\Gamma_{\rm hom}$ components.

temperatures. A temperature dependent plot of the acquired spectra upon illumination with a cw laser of wavelength 633 nm is shown in Fig. 2(a). The optical power density on the sample is kept below 50 μW/μm^2 to avoid any laser induced heating effect. The two conspicuous peaks correspond to the neutral exciton A^0_{1s} and the charged trion A^T_{1s}. The A^0_{1s} peak is fitted with a Voigt function and its constituent Lorentzian component obtained upon deconvolution is the homogeneous part of the total broadening [12,29]. An example is shown in Fig. 2(b) where the experimental data (in symbols) are the acquired spectrum at 3.2 K. The red (orange) line shows the Voigt (Lorentzian) fitting with an FWHM of 5.47(1.92) meV. The variation in the homogeneous ($2\Gamma_{\rm hom}$), inhomogeneous ($2\Gamma_{\rm inhom}$), and the total linewidth of the A^0_{1s} exciton with temperature is shown in Fig. 2(c). The analysis in the following sections is derived from the extracted homogeneous component of the excitonic linewidth only.

When compared to previous experimental data [28,29] and theoretical calculations [33], it is evident that our lowest obtained 1.92 meV homogeneous linewidth is predominantly due to radiative population decay of the excitons. We further affirm this assertion by calculating the photoluminescence spectrum for the limiting case of broadening purely because of fundamental radiative lifetime (as explained later), which has a spectral linewidth ($2\Gamma_{{\rm hom},R}$) of 1.54 meV, as shown in Fig. 2(b) (in green).

IV. SELF-CONSISTENT METHODOLGY TO SEGREGATE RADIATIVE AND NONRADIATIVE LINEWIDTH COMPONENTS

The aim of this section is to segregate the radiative and nonradiative components of the homogeneous exciton linewidth, given an experimentally obtained photoluminescence spectrum. Previous works reported calculation of radiative lifetime of A^0_{1s} exciton assuming zero [34,35] and finite [14] energy broadening in the exciton band. We shall prove in the following text that to obtain the fundamental limits in question, it is important to take into account both the radiative and the nonradiative broadening mechanisms. To achieve this, we propose a self-consistent framework for the calculation of the radiative lifetime of excitons in TMDs. We take $\Gamma(\mathbf{Q}) = \Gamma_R(\mathbf{Q}) + \Gamma_{\rm NR}$, where $\Gamma_R(\mathbf{Q})$ and $\Gamma_{\rm NR}$ are induced by radiative population decay and nonradiative dephasing, respectively, at a given $\mathbf{Q}$. Note that we assume $\Gamma_{\rm NR}$ to be independent of $\mathbf{Q}$.

$\Gamma_R(\mathbf{Q})$ [and hence the exciton radiative lifetime $\tau_R(\mathbf{Q})$] is then given by

$$\Gamma_R(\mathbf{Q}) = \frac{\hbar}{2\tau_R(\mathbf{Q})} = \eta_0 \frac{\hbar e^2}{2m_0^2} |\chi_{\rm ex}(\mathbf{Q})|^2 \times \int_0^\infty dq_z \frac{1}{\sqrt{Q^2+q_z^2}} \times \left(1+\frac{q_z^2}{q_z^2+Q^2}\right) \times \frac{(\Gamma_R(\mathbf{Q})+\Gamma_{\rm NR})/\pi}{\left[E_{\rm ex}(\mathbf{Q}) - \hbar c\sqrt{Q^2+q_z^2}\right]^2 + (\Gamma_R(\mathbf{Q})+\Gamma_{\rm NR})^2}. \quad (2)$$

Here η_0 is the free space impedance and the function $\chi_{\rm ex}(\mathbf{Q})$ is obtained by integrating the quantity $\mathbf{P}_{vc,\mathbf{Q}}(\mathbf{k}).\lambda_{\mathbf{Q}}^{(s)}(\mathbf{k})$ in the $\mathbf{k}$ space [36], where $\mathbf{P}_{vc,\mathbf{Q}}(\mathbf{k})$ is the momentum matrix element between $|v,\mathbf{k}\rangle$ and $|c,\mathbf{k}+\mathbf{Q}\rangle$ [37]. The quasiparticle band-structure for monolayer $MoSe_2$ is obtained using the Lowdin Hamiltonian [38,39]. Details of the Hamiltonian, BS equation and calculation of $|\chi_{\rm ex}(\mathbf{Q})|^2$ are provided in the Supplemental Material Note 1 [40]. The right panel of Fig. 1(d) is a cartoon plot of the decay rate of excitons with energy at different $\mathbf{Q}$ points. We define $I_{\rm cal}^{1s}$ as the calculated homogeneous output of the spontaneous emission from the $1s$ excitons as would be obtained in a PL experiment:

$$I_{\rm cal}^{1s}(E) \propto \sum_{\mathbf{Q}:E\geqslant\hbar cQ} \frac{1}{(\exp^{E_{1s}(\mathbf{Q})/k_BT}-1)} \cdot \frac{1}{\tau_R(E,\mathbf{Q})}. \quad (3)$$

We work in the mathematical framework of Eqs. (2) and (3) put together ensuring that the calculated broadening of $I_{\rm cal}^{1s}$ matches the experimental Lorentzian linewidth of the A_{1s}^0 exciton.

The flow chart in Appendix A explains our proposed methodology for the quantitative estimation of $\Gamma_R(\mathbf{Q})$ and $\Gamma_{\rm NR}$ from $\Gamma_{\rm hom,exp}$ [Fig. 2(c)]. It works in the following way: On starting with an assumed value $\Gamma_{\rm NR}^{(0)}$, the first step is the radiative lifetime calculation. Note that the transcendental nature of Eq. (2) requires solving $\Gamma_R^{(i)}(\mathbf{Q})$ self-consistently for a given $\Gamma_{\rm NR}^{(i)}$, as shown in the right block, where i stands for the iteration index. We next obtain $I_{\rm cal}^{1s}$ [Eq. (3)] with $\tau_R^{(i)}$ calculated for the converged values of $\Gamma_R^{(i)}(\mathbf{Q})$. $\Gamma_{\rm NR}^{(i)}$ is updated appropriately for the successive iterations on comparing the calculated $I_{\rm cal}^{1s}$ linewidth ($2\Gamma_{\rm hom,cal}$) with $2\Gamma_{\rm hom,exp}$. In summary, the left block ensures matching of experimental data with the calculated linewidth and the right block takes into account the necessary self-consistency of Eq. (2) at a given value of $\Gamma_{\rm NR}$.

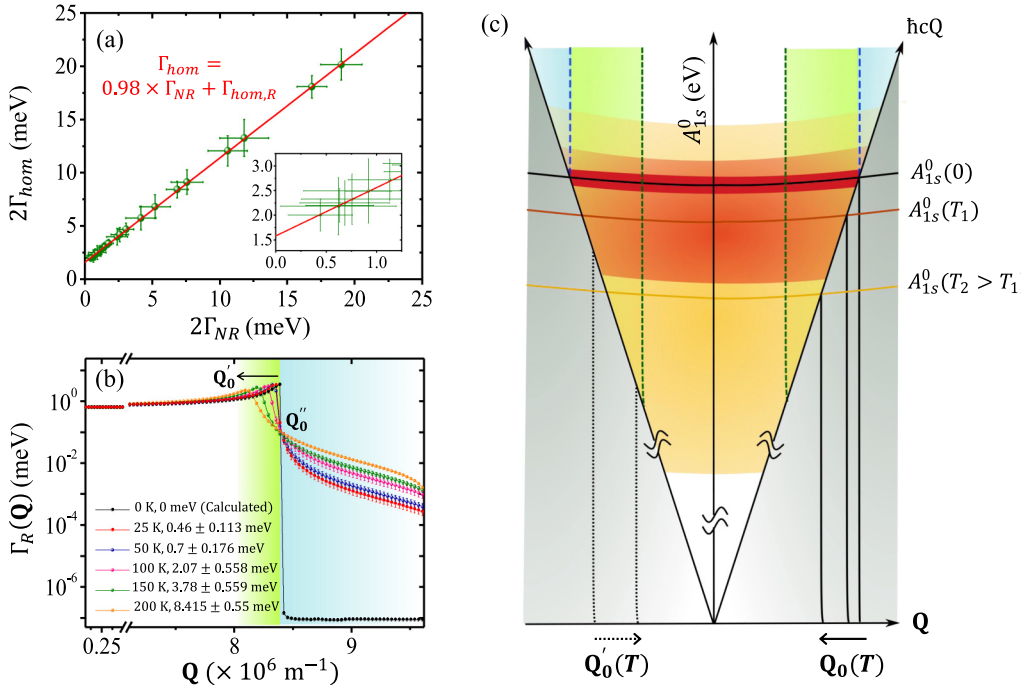

FIG. 3. Temperature dependence of radiative broadening. (a) The homogeneous exciton linewidth $2\Gamma_{\rm hom,exp}$ variation with pure nonradiative linewidth $2\Gamma_{\rm NR}$ (extracted from the experimental data). The (red) line with slope close to unity (~ 0.98) is a good fit to the experimental data. As shown in the inset, an extrapolated value of 1.58 meV at $\Gamma_{\rm NR}=0$ is consistent with the $2\Gamma_{\rm hom,R} = 1.54 \pm 0.17$ meV. (b) Extracted value of $\Gamma_R(\mathbf{Q})$ at different sample temperatures. The value of $\Gamma_{\rm NR}$ at the corresponding temperature is mentioned in the legend. $\Gamma_R(\mathbf{Q})$ is maximum at $\mathbf{Q_0'}$ and the curves converge at $\mathbf{Q_0''}$ irrespective of T. (c) Schematic representation of the light cone for three different temperatures $0 < T_1 < T_2$ with the increasing broadening indicated by red, orange, and yellow shades. With an increase in T, optical band gap reduces and both $\mathbf{Q_0}$ and $\mathbf{Q_0'}$ shift towards $\mathbf{Q}=\mathbf{0}$. The color coding of different regions in $\mathbf{Q}$ correspond to (b), namely, white ($\mathbf{Q} < \mathbf{Q_0'}$), green ($\mathbf{Q_0'} < \mathbf{Q} < \mathbf{Q_0''}$), and blue ($\mathbf{Q} > \mathbf{Q_0''}$).

V. DISCUSSIONS

A. Fundamental limit of radiative linewidth

The self-consistent nature of Eq. (2) becomes more important when $\Gamma_R(\mathbf{Q})$ is comparable to or larger than Γ_{NR}. This is precisely the case for monolayer TMDs at low temperature and at low excitation density. In the limiting case of $\Gamma_{\mathrm{NR}} \ll \Gamma_R(\mathbf{Q})$, we can solve for $\Gamma_R(\mathbf{Q})$ independently from Eq. (2). This leads to a fundamental homogeneous emission linewidth of 1.54 ± 0.17 meV as shown by the green line in Fig. 2(b). This shows that the exciton Hamiltonian is sufficiently non-Hermitian due to the fast exciton radiative decay [41], thereby validating the need for such a self-consistent approach for determining the exciton radiative lifetime even in the absence of any nonradiative scattering process. The error bar takes into account a $\pm 5\%$ variation in the Lowdin Hamiltonian parameters and sensitivity of $\mathbf{k}$ space griding in calculating $|\chi_{\mathrm{ex}}(\mathbf{Q})|^2$ [42]. Note that the technique is an extremely powerful tool to obtain the fundamental radiative linewidth as it does not require any broadening to be introduced "by hand," as is usually done in most calculations, rather it self-consistently takes care of the radiative component of the homogeneous broadening.

The variation in Γ_{hom} as a function of the extracted Γ_{NR} at each temperature using the proposed algorithm is plotted in Fig. 3(a). The data points track closely a reference line of slope ~ 0.98 as shown in the figure, thus affirming the nonradiative nature of the homogeneous linewidth at all temperatures. The inset plot is a zoomed in view that shows, on extrapolation, a residual radiative linewidth of 1.58 meV corresponding to $\Gamma_{\mathrm{NR}} = 0$. This is consistent with our calculated fundamental linewidth value of 1.54 ± 0.17 meV.

B. Temperature dependence of radiative linewidth—inside and outside light cone

Figure 3(b) illustrates the temperature induced variation in the self-consistently obtained $\mathbf{Q}$ resolved Γ_R. The corresponding values of the extracted Γ_{NR} is shown in the legend. For reference, the limiting case of purely radiative linewidth at $T = 0\,\mathrm{K}$ and $\Gamma_{\mathrm{NR}} = 0\,\mathrm{meV}$ is shown in black. $\Gamma_R(\mathbf{Q})$ shows a strongly nonmonotonic behavior with $\mathbf{Q}$, reaching its maximum value at $\mathbf{Q_0'}$. The color shades represent the different characteristic regions. $\Gamma_R(\mathbf{Q})$ is almost invariant for the most part of $\mathbf{Q} < \mathbf{Q_0'}$ points within the light cone (white region). With an increase in temperature, $\mathbf{Q_0'}$ shifts towards $\mathbf{Q} = \mathbf{0}$. This can be understood as a competition between two temperature dependent effects, namely a reduction in the optical band gap (A_{1s}^0) and an increase in Γ_{NR} with T. This is schematically explained in Fig. 3(c) for three different temperatures with $0 < T_1 < T_2$. For $\mathbf{Q_0'} < \mathbf{Q} < \mathbf{Q_0''}$ (green shade), owing to larger Γ_{NR} at higher T, a larger fraction of the states lie below the light line, which manifests as a strong suppression in $\Gamma_R(\mathbf{Q})$. All the curves converge to a point $\mathbf{Q_0''} \approx \mathbf{Q_0}(0)$, before diverging again in the blue region. Note that, the contribution of the state $\mathbf{Q_0}(T)$ remains 50% irrespective of temperature. For $\mathbf{Q} > \mathbf{Q_0''}$ (blue region), $\Gamma_R(\mathbf{Q})$ experiences a significant increment at higher T as more excitonic states appear above the light line $\hbar cQ$, which are otherwise forbidden in the case of negligible broadening. The variation of $\Gamma_R(\mathbf{Q})$ as a function of temperature is explained in Supplemental Material Note 2 [40]

C. Nonradiative linewidth broadening and its fundamental limit

The extracted Γ_{NR} is plotted in Fig. 4(a) (symbols) as a function of temperature. Such a strong temperature dependence is well described by exciton-phonon scattering processes [33,43]. As the radiative emission process is a result of recombination of excitons $\mathbf{Q} \approx \mathbf{0}$, one usually assumes that only phonon absorption processes are allowed [44]. However, in the presence of large radiative broadening of the excitonic states, the low energy (close to zone-center) acoustic phonon emission process is allowed within the light cone, apart from the usual absorption processes of acoustic and

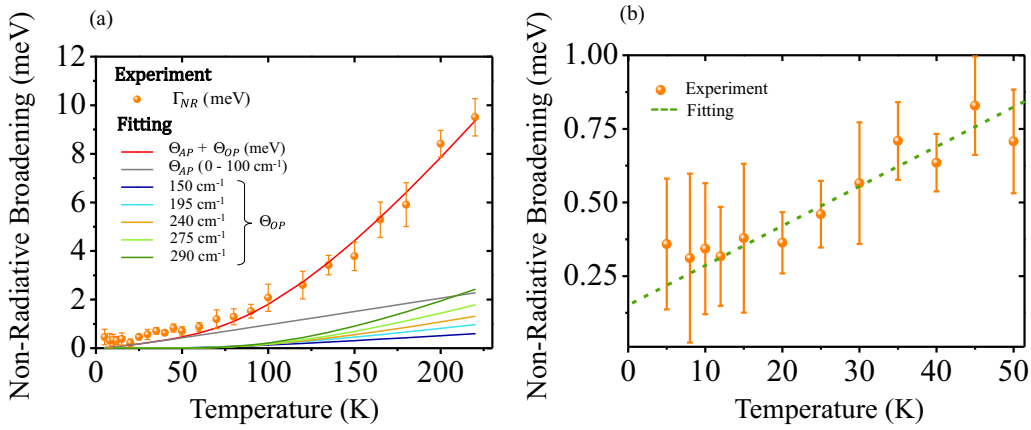

FIG. 4. Nonradiative broadening due to exciton-phonon coupling and zero-point energy. (a) Extracted Γ_{NR} (orange symbols with error bars) and the fitted curve (red line) using a combination of Θ_{AP} (acoustic phonon emission and absorption) and Θ_{OP} (optical phonon absorption) terms from Eq. (4). The individual contribution of acoustic and optical phonons is also shown separately. (b) Zoomed-in view of the low temperature regime [$T < 50\,\mathrm{K}$]. The green dashed line shows a linear fit with a slope of 13.56 $\mu\mathrm{eV\,K^{-1}}$ and a vertical intercept at $T = 0\,\mathrm{K}$ being $\Gamma_{\mathrm{NR}}(0) = 150$ μeV. This indicates a large fundamental nonradiative linewidth broadening due to zero-point energy of acoustic phonons.

optical phonons. Therefore, the temperature dependence of the induced nonradiative broadening is given by

$$\Gamma_{\rm NR}^{\rm cal} = \sum_{\Omega_{\rm AP}} C_{\rm AP}\,[2N(\Omega_{\rm AP},T)+1] + \sum_{\Omega_{\rm OP}} C_{\rm OP}\,N(\Omega_{\rm OP},T) \tag{4}$$

$$= \underbrace{\sum_{\Omega_{\rm AP}} C_{\rm AP}}_{\Theta_0} + \underbrace{\sum_{\Omega_{\rm AP}} 2C_{\rm AP}\,N(\Omega_{\rm AP},T)}_{\Theta_{\rm AP}} + \underbrace{\sum_{\Omega_{\rm OP}} C_{\rm OP}\,N(\Omega_{\rm OP},T)}_{\Theta_{\rm OP}}. \tag{5}$$

Here N denotes the Bose occupation number given by $N(\Omega,T) = (e^{\frac{\hbar\Omega}{k_B T}} - 1)^{-1}$. The combination of the second and the third terms in Eq. (5) is shown in the red line in Fig. 4(a), showing good agreement with the data at temperature higher than 50 K. We take $\Omega_{\rm AP}$ values for modes in the acoustic branch up to 100 $\rm cm^{-1}$ with a fitted coupling strength $C_{\rm AP} = 162.5\ \mu$eV. $\Omega_{\rm OP}$ corresponds to specific optical modes of frequency 150, 195, 240, 275, and 290 $\rm cm^{-1}$ with coupling strength $C_{\rm OP} = 1, 2.5, 5, 9$, and 13.75 meV, respectively. The individual mode contributions to $\Gamma_{\rm NR}$ is also shown in the same plot. The acoustic phonon branch contributes almost linearly to $\Gamma_{\rm NR}$ whereas the optical modes are responsible for the superlinear increase in broadening at higher temperatures.

At lower temperatures ($T < 50$ K), we observe a large deviation between the extracted $\Gamma_{\rm NR}$ and the fitted line using $\Theta_{\rm AP} + \Theta_{\rm OP}$ from Eq. (5). This residual broadening can originate from multiple nonradiative channels, such as excitation induced (for example, exciton-free carrier scattering [44,45] and exciton-exciton scattering [33,44,45]) and spin flip induced dephasing. The spin flipping time being on the order of nanosecond [46] can only provide a linewidth broadening of a few μeV and can be safely ignored. We also note that our measurements are performed at a low excitation density of $N_x < 9\times10^8$ $\rm cm^{-2}$ (an upper limit on the exciton density assuming 100% quantum yield). In addition, excitation induced broadening ($\propto a_B^2 E_b N_x$ where a_B is the Bohr radius and E_b is the binding energy) is suppressed in the case of the A_{1s}^0 exciton for monolayer TMDs due to small a_B (less than a nanometer). We estimate an overall linewidth broadening of only $\sim$2.4 μeV due to excitation induced broadening. Further, we discard any contribution of exciton-free carrier scattering in the homogeneous exciton linewidth due to the absence of a uniform free carrier density in monolayer $MoSe_2$ at low sample temperature. Note that the origin of the trion peak in Fig. 2(a) is only a result of inhomogeneous local doping effect induced charge puddles due to charge fluctuations in the SiO_2 substrate. This is verified by the complete Gaussian (and hence inhomogeneous) nature of the line shape of the trion peak. Therefore, any scattering with the localized charge carriers only affects the inhomogeneous broadening of the exciton linewidth, leaving the homogeneous linewidth component unaffected.

We understand the observed deviation at low temperature as the contribution of zero point energy of the acoustic phonons, as described by the first term (Θ_0) in Eq. (5). At low temperature, following the approach of Marini [47], we obtain a quantitative expression for $\Gamma_{\rm NR}$ given by $\Gamma_{\rm NR}(T) = \alpha(\frac{E_0}{2k_B} + T)$, where E_0 is roughly equal to the broadening of the exciton band (derivation in Appendix B). On putting $E_0 = 2(\Gamma_{{\rm hom},R} + \Gamma_{\rm NR}(0))$, we obtain the fundamental non-radiative linewidth at $T = 0$ K by

$$\Gamma_{\rm NR}(0) = \alpha\left(\frac{E_0}{2k_B}\right) \tag{6}$$

$$= \alpha\left(\frac{\Gamma_{{\rm hom},R} + \Gamma_{\rm NR}(0)}{k_B}\right) \tag{7}$$

$$= \frac{\alpha'}{1-\alpha'}\Gamma_{{\rm hom},R}, \quad \left(\alpha' = \frac{\alpha}{k_B}\right). \tag{8}$$

The low temperature regime is shown separately in Fig. 4(b). The slope of $\Gamma_{\rm NR}$ versus T gives an estimate of $\alpha \approx 13.56\ \mu{\rm eV\,K^{-1}}$. Using the relation in Eq. (8) and putting the value of $\Gamma_{{\rm hom},R}$ as 1.54 meV, this readily allows us to obtain $\Gamma_{\rm NR}(0) \approx 134\ \mu$eV. In the light of the negligible contribution due to spin-flip and excitation induced dephasing, this is in excellent agreement with the intercept of 150 μeV of the fitted dashed line at $T = 0$ in Fig. 4(b). This allows us to validate the assertion of large linewidth broadening resulting from zero-point energy and results in a fundamental nonradiative exciton linewidth broadening of $\sim$0.27 meV. An increase in the radiative linewidth directly enhances the zero-point broadening, as suggested by the strong correlation between the two quantities in Eq. (8).

VI. CONCLUSION

In summary, we investigated the principal factors that determine the fundamental limit of excitonic linewidth in monolayer TMDs—a class of systems that exhibit extremely short radiative spontaneous decay of strongly bound excitons. We showed that the large broadening of the excitonic states due to the strong radiative dephasing must be incorporated in the light cone picture in a self-consistent way for accurate estimation of the emission linewidth. We proposed a powerful technique to segregate the individual radiative and nonradiative components of the linewidth. This self-consistent approach sets a limit of 1.54 meV on the fundamental radiative linewidth. One striking observation of this limit is that the zero-point energy induced broadening, which determines the fundamental limit of the nonradiative broadening is extraordinarily large ($\sim$0.27 meV)—a manifestation of the large radiative broadening that allows the acoustic phonon emission process at the ultralow temperature regime. The results presented in this work are robust against the inhomogeneity of the sample as long as the factors that cause inhomogeneous broadening does not affect the homogeneous linewidth. The findings advance the microscopic understanding of light emission governed by tightly bound excitons in layered semiconductors and can pave way for novel optoelectronic device concepts, including exploitation of strong coupling regime of light-matter interaction.

ACKNOWLEDGMENTS

This work was supported, in part, by a grant under Indian Space Research Organization (ISRO), by the grants under Ramanujan Fellowship, Early Career Award, and Nano

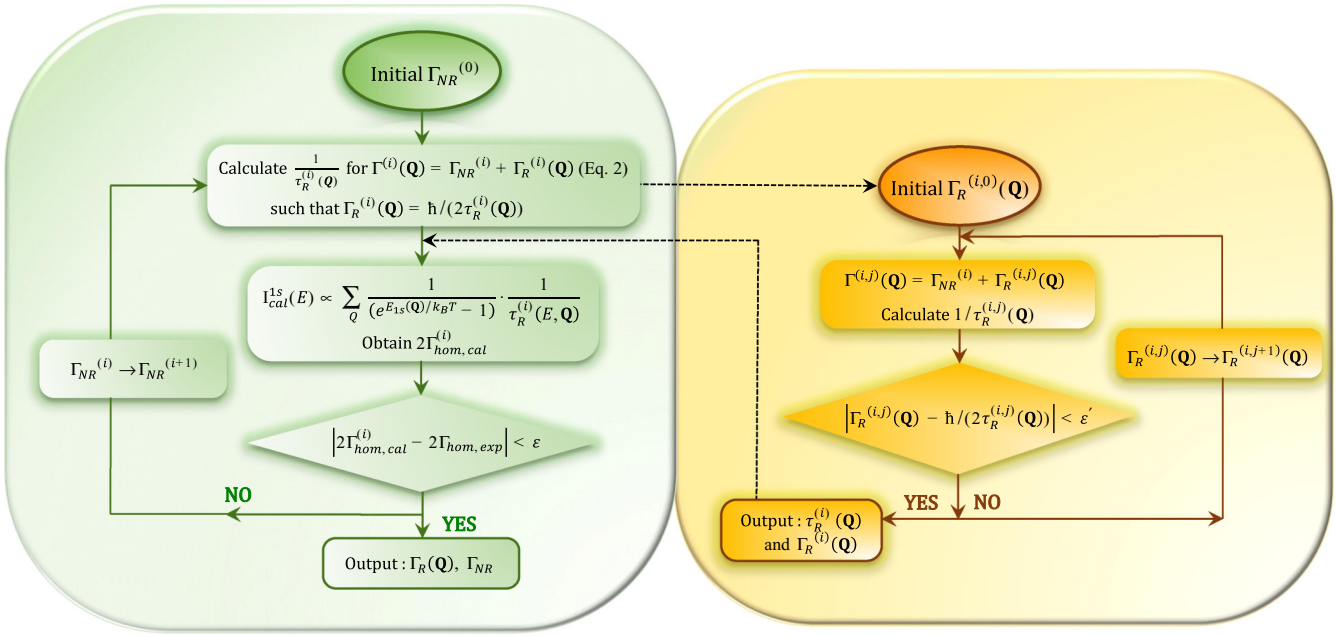

FIG. 5. Flow chart of the algorithm for calculation of radiative and nonradiative components of homogeneous linewidth.

Mission from the Department of Science and Technology (DST), and by a grant from MHRD, MeitY and DST Nano Mission through NNetRA. The authors declare no competing financial interest.

APPENDIX A

The algorithm employed for calculating exciton radiative lifetime ($\tau_R(\mathbf{Q})$) by deconvoluting the $\mathbf{Q}$ resolved radiative $\Gamma_R(\mathbf{Q})$ and nonradiative $\Gamma_{\rm NR}$ components, given a homogeneous linewidth obtained from experiment ($2\Gamma_{\rm hom,exp}$). The methodology is explained with the help of a flowchart in Fig. 5. The convergence of the right block ensures a self-consistent $\Gamma_R(\mathbf{Q})$ for a given $\Gamma_{\rm NR}$ [Eq. (2)]. The left block finds the fitted value of $\Gamma_{\rm NR}$ for a given experimentally obtained spectral linewidth of the exciton line. $\Gamma_{\rm NR}$ is the only fitting parameter in the algorithm.

APPENDIX B

The temperature induced broadening of the exciton bands arising due to exciton-phonon scattering [47] is given by

$$\Gamma_{\rm NR}(T) = {\rm Im}[E_s(T)] = \int d\omega\, {\rm Im}[g^2F_s(\omega,T)]\left[N(\omega,T) + \frac{1}{2} \pm \frac{1}{2}\right]. \tag{B1}$$

The upper and the lower signs correspond to phonon emission and absorption processes, respectively. $g^2F_s(\omega,T) = \sum_{v,c,\mathbf{k}} |\lambda^{(s)}(\mathbf{k},T)|^2[g^2F_{c,\mathbf{k}}(\omega) - g^2F_{v,\mathbf{k}}(\omega)]$ is the exciton-phonon coupling function. We consider contribution from only the lowermost conduction band and the topmost valence band for monolayer $MoSe_2$

$$g^2F_{c,\mathbf{k}}(\omega) - g^2F_{v,\mathbf{k}}(\omega) = \sum\left(\frac{\partial\epsilon_{c,\mathbf{k}}}{\partial N(\omega_\nu,T)} - \frac{\partial\epsilon_{v,\mathbf{k}}}{\partial N(\omega_\nu,T)}\right)\delta(\omega-\omega_\nu) \tag{B2}$$

$$\approx \sum \frac{\partial\epsilon_{g,\mathbf{k}}}{\partial N(\omega_\nu,T)}\delta(\omega-\omega_\nu), \tag{B3}$$

where the summation runs for all the phonon modes and $\epsilon_{g,\mathbf{k}} = \epsilon_{c,\mathbf{k}} - \epsilon_{v,\mathbf{k}}$

$$\Gamma_{\rm NR}(T) = \sum_{\nu,\omega_\nu} {\rm Im}\left[\sum_{\mathbf{k}} |\lambda^{(s)}(\mathbf{k},T)|^2 \frac{\partial\epsilon_{g,\mathbf{k}}}{\partial N(\omega_\nu,T)}\right] \times \left(N(\omega_\nu,T) + \frac{1}{2} \pm \frac{1}{2}\right). \tag{B4}$$

We use the shorthand notation $\beta_{\omega_\nu}(T) = {\rm Im}[\sum_{\mathbf{k}} |\lambda^{(s)}(\mathbf{k},T)|^2 \frac{\partial\epsilon_{g,\mathbf{k}}}{\partial N(\omega_\nu,T)}]$, quantifying the coupling strength of excitons to phonon mode ν, ω_ν at T. $\lambda^s(\mathbf{k},T)$ is the BSE solution of the non-Hermition exciton Hamiltonian, the temperature dependence arising as a result of quasiparticle bands broadening due to electron phonon scattering. The exciton phonon scattering does not vanish even at $T = 0\,{\rm K}$, as $N \rightarrow 0$, due to scattering via phonon emission process and induces finite zero point broadening in the exciton band.

To quantify $\Gamma_{\rm NR}$ due to zone center acoustic phonon emission at low temperatures, we approximate for analytical purpose, that the coupling coefficient $\beta_{\omega_\nu}(T)$ is invariant with ω_ν, T and replace $\beta_{\omega_\nu}(T)$ by β. On putting $N \approx \frac{k_BT}{\hbar\omega_\nu}$ for the

acoustic phonon modes at small temperatures, we get

$$\Gamma_{\mathrm{NR}}(T) = \beta \sum_{\omega_\nu} \left(\frac{k_B T}{\hbar \omega_\nu} + 1 \right)$$
$$= \frac{\beta A N_b}{2\pi} \int_0^{q_0} dq\, q \left(\frac{k_B T}{\hbar c q} + 1 \right) (\hbar \omega_\nu = \hbar c q)$$
$$= \frac{\beta A N_b}{2\pi} \left(\frac{q_o^2}{2} + \frac{k_B}{\hbar c} q_o T \right) = \alpha \left(\frac{E_0}{2k_B} + T \right).$$

Here $\alpha = \frac{\beta A N_b k_B q_0}{2\pi \hbar c}$ and $E_0 = \hbar c q_0$. E_0 and q_0 is defined in Fig. 6, where E_0 is qualitatively of the same order as the broadening of the exciton band. N_b quantifies the number of phonon branches and are taken to be contributing identically. A is the sample area.

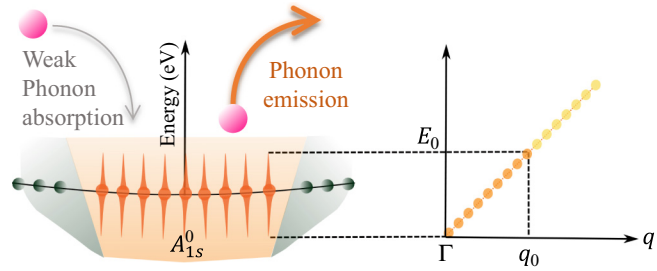

FIG. 6. Nonradiative broadening due to phonon emission as $\mathbf{T} \to \mathbf{0}$. Acoustic modes upto $E_0 (= \hbar c q_0)$ contribute to Γ_{NR} in the exciton band. Phonon emission is the dominant scattering mechanism (orange arrow) as phonon absorption (grey arrow) is a weak process at small temperatures.

[1] Z. Ye, T. Cao, K. O'Brien, H. Zhu, X. Yin, Y. Wang, S. G. Louie, and X. Zhang, Probing excitonic dark states in single-layer tungsten disulphide, Nature **513**, 214 (2014).

[2] K. He, N. Kumar, L. Zhao, Z. Wang, K. F. Mak, H. Zhao, and J. Shan, Tightly Bound Excitons in Monolayer WSe_2, Phys. Rev. Lett. **113**, 026803 (2014).

[3] J. S. Ross, S. Wu, H. Yu, N. J. Ghimire, A. M. Jones, G. Aivazian, J. Yan, D. G. Mandrus, D. Xiao, W. Yao, and X. Xu, Electrical control of neutral and charged excitons in a monolayer semiconductor, Nat. Commun. **4**, 1474 (2013).

[4] T. C. Berkelbach, M. S. Hybertsen, and D. R. Reichman, Theory of neutral and charged excitons in monolayer transition metal dichalcogenides, Phys. Rev. B **88**, 045318 (2013).

[5] A. Chernikov, T. C. Berkelbach, H. M. Hill, A. Rigosi, Y. Li, O. B. Aslan, D. R. Reichman, M. S. Hybertsen, and T. F. Heinz, Exciton Binding Energy and Nonhydrogenic Rydberg Series in Monolayer WS_2, Phys. Rev. Lett. **113**, 076802 (2014).

[6] H. M. Hill, A. F. Rigosi, C. Roquelet, A. Chernikov, T. C. Berkelbach, D. R. Reichman, M. S. Hybertsen, L. E. Brus, and T. F. Heinz, Observation of excitonic rydberg states in monolayer MoS_2 and WS_2 by photoluminescence excitation spectroscopy, Nano Lett. **15**, 2992 (2015).

[7] G. Gupta, S. Kallatt, and K. Majumdar, Direct observation of giant binding energy modulation of exciton complexes in monolayer $MoSe_2$, Phys. Rev. B **96**, 081403 (2017).

[8] K. Hao, J. F. Specht, P. Nagler, L. Xu, K. Tran, A. Singh, C. K. Dass, C. Schüller, T. Korn, M. Richter, A. Knorr, X. Li, and G. Moody, Neutral and charged inter-valley biexcitons in monolayer $MoSe_2$, Nat. Commun. **8**, 15552 (2017).

[9] X. Liu, T. Galfsky, Z. Sun, F. Xia, E.-c. Lin, Y.-H. Lee, S. Kéna-Cohen, and V. M. Menon, Strong light–matter coupling in two-dimensional atomic crystals, Nat. Photon. **9**, 30 (2015).

[10] A. Amo, T. C. H. Liew, C. Adrados, R. Houdré, E. Giacobino, A. V. Kavokin, and A. Bramati, Exciton–polariton spin switches, Nat. Photon. **4**, 361 (2010).

[11] C. M. Chow, H. Yu, A. M. Jones, J. R. Schaibley, M. Koehler, D. G. Mandrus, R. Merlin, W. Yao, and X. Xu, Phonon-assisted oscillatory exciton dynamics in monolayer $MoSe_2$, npj 2D Mater. Appl. **1**, 33 (2017).

[12] M. Engel and M. Steiner, Room-temperature quantum-confined stark effect in atomically thin semiconductor, arXiv:1802.03003.

[13] C. Robert, D. Lagarde, F. Cadiz, G. Wang, B. Lassagne, T. Amand, A. Balocchi, P. Renucci, S. Tongay, B. Urbaszek, and X. Marie, Exciton radiative lifetime in transition metal dichalcogenide monolayers, Phys. Rev. B **93**, 205423 (2016).

[14] H. Wang, C. Zhang, W. Chan, C. Manolatou, S. Tiwari, and F. Rana, Radiative lifetimes of excitons and trions in monolayers of the metal dichalcogenide MoS_2, Phys. Rev. B **93**, 045407 (2016).

[15] C.-K. Sun, S. Keller, G. Wang, M. S. Minsky, J. E. Bowers, and S. P. DenBaars, Radiative recombination lifetime measurements of ingan single quantum well, Appl. Phys. Lett. **69**, 1936 (1996).

[16] T. J. Badcock, M. Ali, T. Zhu, M. Pristovsek, R. A. Oliver, and A. J. Shields, Radiative recombination mechanisms in polar and non-polar InGaN/GaN quantum well Led structures, Appl. Phys. Lett. **109**, 151110 (2016).

[17] S. K. Goswami, T. S. Kim, E. Oh, K. K. Challa, and E.-T. Kim, Optical properties and effect of carrier tunneling in cdse colloidal quantum dots: A comparative study with different ligands, AIP Adv. **2**, 032132 (2012).

[18] N. Bel Haj Mohamed, M. Haouari, Z. Zaaboub, M. Nafoutti, F. Hassen, H. Maaref, and H. B. Ouada, Time resolved and temperature dependence of the radiative properties of thiol-capped cds nanoparticles films, J. Nanopart. Res. **16**, 2242 (2014).

[19] M. Califano, A. Zunger, and A. Franceschetti, Direct carrier multiplication due to inverse auger scattering in CdSe quantum dots, Appl. Phys. Lett. **84**, 2409 (2004).

[20] F. F. So and S. R. Forrest, Evidence for Exciton Confinement in Crystalline Organic Multiple Quantum Wells, Phys. Rev. Lett. **66**, 2649 (1991).

[21] V. Perebeinos, J. Tersoff, and P. Avouris, Radiative lifetime of excitons in carbon nanotubes, Nano Lett. **5**, 2495 (2005).

[22] Y. Ouyang, D. Mann, H. Dai, and J. Guo, Theoretical investigations on thermal light emission from metallic carbon nanotubes, IEEE Trans. Nanotechnol. **6**, 682 (2007).

[23] C. D. Spataru, S. Ismail-Beigi, R. B. Capaz, and S. G. Louie, Theory and *Ab Initio* Calculation of Radiative Lifetime of Excitons in Semiconducting Carbon Nanotubes, Phys. Rev. Lett. **95**, 247402 (2005).

[24] A. Splendiani, L. Sun, Y. Zhang, T. Li, J. Kim, C.-Y. Chim, G. Galli, and F. Wang, Emerging photoluminescence in monolayer MoS_2, Nano lett. **10**, 1271 (2010).

[25] A. Steinhoff, J.-H. Kim, F. Jahnke, M. Roösner, D.-S. Kim, Ch. Lee, G. H. Han, M. S. Jeong, T. O. Wehling, and C. Gies, Efficient excitonic photoluminescence in direct and indirect band gap monolayer MoS_2, Nano Lett. **15**, 6841 (2015).

[26] R. Cheng, D. Li, H. Zhou, C. Wang, A. Yin, S. Jiang, Y. Liu, Yu. Chen, Yu. Huang, and X. Duan, Electroluminescence and photocurrent generation from atomically sharp Wse_2/MoS_2 heterojunction *p–n* diodes, Nano Lett. **14**, 5590 (2014).

[27] R. S. Sundaram, M. Engel, A. Lombardo, R. Krupke, A. C. Ferrari, P. H. Avouris, and M. Steiner, Electroluminescence in single layer MoS_2, Nano Lett. **13**, 1416 (2013).

[28] O. A. Ajayi, J. V. Ardelean, G. D. Shepard, J. Wang, A. Antony, T. Taniguchi, K. Watanabe, T. F. Heinz, S. Strauf, X. Y. Zhu, and J. C. Hone, Approaching the intrinsic photoluminescence linewidth in transition metal dichalcogenide monolayers, 2D Mater. **4**, 031011 (2017).

[29] F. Cadiz, E. Courtade, C. Robert, G. Wang, Y. Shen, H. Cai, T. Taniguchi, K. Watanabe, H. Carrere, D. Lagarde, M. Manca, T. Amand, P. Renucci, S. Tongay, X. Marie, and B. Urbaszek, Excitonic Linewidth Approaching the Homogeneous Limit in MoS_2-Based Van Der Waals Heterostructures, Phys. Rev. X **7**, 021026 (2017).

[30] G. D. Shepard, J. V. Ardelean, O. A. Ajayi, D. Rhodes, X. Zhu, J. C. Hone, and S. Strauf, Trion-species-resolved quantum beats in $MoSe_2$, ACS Nano **11**, 11550 (2017).

[31] F. Wu, F. Qu, and A. H. MacDonald, Exciton band structure of monolayer MoS_2, Phys. Rev. B **91**, 075310 (2015).

[32] D. Y. Qiu, T. Cao, and S. G. Louie, Nonanalyticity, Valley Quantum Phases, and Lightlike Exciton Dispersion in Monolayer Transition Metal Dichalcogenides: Theory and First-Principles Calculations, Phys. Rev. Lett. **115**, 176801 (2015).

[33] A. Singh, A. Knorr, C. K. Dass, C.-H. Chen, E. Malic, G. Moody, G. Clark, G. Berghäuser, K. Hao, K. Tran, G. Clark, X. Xu, G. Berghäuser, E. Malic, A. Knorr, and X. Li, Intrinsic homogeneous linewidth and broadening mechanisms of excitons in monolayer transition metal dichalcogenides, Nat. Commun. **6**, 8315 (2015).

[34] M. Palummo, M. Bernardi, and J. C. Grossman, Exciton radiative lifetimes in two-dimensional transition metal dichalcogenides, Nano Lett. **15**, 2794 (2015).

[35] H.-Y. Chen, M. Palummo, D. Sangalli, and M. Bernardi, Theory and *ab initio* computation of the anisotropic light emission in monolayer transition metal dichalcogenides, Nano Lett. **18**, 3839 (2018).

[36] C. Zhang, H. Wang, W. Chan, C. Manolatou, and F. Rana, Absorption of light by excitons and trions in monolayers of metal dichalcogenide MoS_2: Experiments and theory, Phys. Rev. B **89**, 205436 (2014).

[37] D. Xiao, G.-B. Liu, W. Feng, X. Xu, and W. Yao, Coupled Spin and Valley Physics in Monolayers of Mos_2 and Other Group-VI Dichalcogenides, Phys. Rev. Lett. **108**, 196802 (2012).

[38] A. Kormányos, G. Burkard, M. Gmitra, J. Fabian, V. Zólyomi, N. D. Drummond, and V. Fal'ko, k.p theory for two-dimensional transition metal dichalcogenide semiconductors, 2D Mater. **2**, 022001 (2015).

[39] A. Kormányos, V. Zólyomi, N. D. Drummond, P. Rakyta, G. Burkard, and V. I. Fal'ko, Monolayer MoS_2: Trigonal warping, the γ valley, and spin-orbit coupling effects, Phys. Rev. B **88**, 045416 (2013).

[40] See Supplemental Material at http://link.aps.org/supplemental/10.1103/PhysRevB.99.085412 for exciton bandstructure calculation in $MoSe_2$ and effect of temperature on radiative broadening.

[41] A. Molina-Sánchez, M. Palummo, A. Marini, and L. Wirtz, Temperature-dependent excitonic effects in the optical properties of single-layer MoS_2, Phys. Rev. B **93**, 155435 (2016).

[42] D. Y. Qiu, H. Felipe, and S. G. Louie, Optical Spectrum of MoS_2: Many-Body Effects and Diversity of Exciton States, Phys. Rev. Lett. **111**, 216805 (2013).

[43] M. Selig, G. Berghäuser, A. Raja, P. Nagler, C. Schüller, T. F. Heinz, T. Korn, A. Chernikov, E. Malic, and A. Knorr, Excitonic linewidth and coherence lifetime in monolayer transition metal dichalcogenides, Nat. Commun. **7**, 13279 (2016).

[44] R. Hellmann, M. Koch, J. Feldmann, S. T. Cundiff, E. O. Göbel, D. R. Yakovlev, A. Waag, and G. Landwehr, Homogeneous linewidth of excitons in semimagnetic $CdTe/Cd_{1-x}Mn_x$ te multiple quantum wells, Phys. Rev. B **48**, 2847 (1993).

[45] A. Honold, L. Schultheis, J. Kuhl, and C. W. Tu, Collision broadening of two-dimensional excitons in a gaas single quantum well, Phys. Rev. B **40**, 6442 (1989).

[46] L. Yang, N. A. Sinitsyn, W. Chen, J. Yuan, J. Zhang, J. Lou, and S. A. Crooker, Long-lived nanosecond spin relaxation and spin coherence of electrons in monolayer MoS_2 and Ws_2, Nat. Phys. **11**, 830 (2015).

[47] A. Marini, *Ab Initio* Finite-Temperature Excitons, Phys. Rev. Lett. **101**, 106405 (2008).